Journal of Computational and Applied Mathematics 340 (2018) 653–663

Contents lists available at ScienceDirect

Journal of Computational and Applied Mathematics

journal homepage: www.elsevier.com/locate/cam

Buckling analysis of geometrically nonlinear curved beams

S. Stoykov

Institute of Information and Communication Technologies, Bulgarian Academy of Sciences, Acad. G. Bonchev str., bl. 25A, 1113 Sofia, Bulgaria

ARTICLE INFO

Article history:
Received 7 June 2017
Received in revised form 31 August 2017

Keywords:
Parametrical analysis
Stability
Continuation method
Bifurcation points

ABSTRACT

The equation of motion of curved beams is derived in polar coordinate system which represents exactly the geometry of the beam. The displacements of the beam in radial and circumferential directions are expressed by assuming Bernoulli–Euler's theory. The nonlinear strain–displacement relations are obtained from the Green–Lagrange strain tensor written in cylindrical coordinate system, but only the components related with radial and circumferential displacements are used. The equation of motion is derived by the principle of virtual work and it is discretized into a system of ordinary differential equations by Ritz method. Static analysis is performed in parametrical domain, assuming the magnitude of the applied force as parameter, and stability of the solution is determined. The nonlinear system of equations is solved by Newton–Raphson's method. Prediction for the next point from the force–displacement curve is defined by the arc-length continuation method. Bifurcation points are found and the corresponding secondary branches with the deformed shapes are obtained and presented.

1. Introduction

Curved beams are structural elements with variety of applications among engineering constructions. Curved beams have application in modern bridges, they are also used in the design of light-weight roof structures or in composite components of engineering structures, like helicopter blades or wind turbine blades. The increasing use of curved beams demands accurate mathematical models to perform their analysis and to understand their behavior.

The most popular approach for modeling curved structures is by the finite element method. Majority of the research is based on straight beam elements. This approach is sufficiently accurate for slender curved beams, for which the product of the initial curvature and the height of the beam is much smaller than unity. When this product is not small, the strains of curved beams are much different than the strains of straight beams [1]. The circumferential strain varies linearly with the distance from the center of the cross section for straight beams, but does not vary linearly for curved beams. Thus, additional considerations should be taken into account for achieving better mathematical models of curved beams.

Some of the most common models of curved beams in the literature are shortly referenced here. The differential equations of elastic, curved beams with un-symmetric axes were derived in Cartesian coordinates in [2] and free vibrations were analyzed. The authors extended the derived beam model by including the effects of axial extension, shear deformation, and rotatory inertia [3]. Linear static analysis of orthotropic functionally graded curved beams was performed in [4]. The equilibrium equations were derived in polar coordinate system. Buckling of curved beams was analyzed in [5]. The authors used transformation from curvilinear coordinate to local coordinate for representing the curvature of the beam.

A hierarchical finite element for curved thick beams was developed in [6]. Geometrical nonlinearity was included in the model and nonlinear vibrations were investigated in time domain. A co-rotational finite element formulation for modeling

E-mail address: stoykov@parallel.bas.bg.

http://dx.doi.org/10.1016/j.cam.2017.08.028
0377-0427/

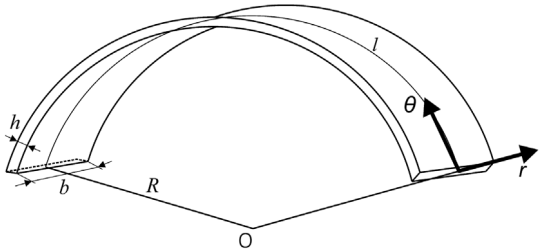

Fig. 1. Geometry of curved beam in polar coordinate system.

curved beams by assuming Bernoulli–Euler's theory was developed in [7]. The deformational nodal forces were derived by consistent linearization of the geometrically nonlinear beam theory.

Three-dimensional displacement components of curved beams were derived in cylindrical coordinate system in [8]. The authors considered torsion and warping deformations of the cross section, and investigated linear static behavior of the beam with different cross sections. Thermo-elastic vibrations of curved beams were analyzed in [9]. The influence of the temperature and ratio of curvature were investigated and periodic and non-periodic vibrations were found. Free and forced vibrations of curved nanobeams were investigated by nonlocal elasticity beam theory [10]. The effects of several parameters like thickness ratio, beam length, curvature of the beam on the dynamic response were investigated. Mixed finite element for curved beams was developed in [11] based on geometrically exact beam theory. More recent works on development and analysis of curved beams can be found, for example in [12–17].

In the current work, the equilibrium equation of curved beam is derived in polar coordinate system. This approach allows one to model exactly the initial curvature of the beam. Bernoulli–Euler hypothesis for thin beams is expressed in polar coordinate system. Geometrical type of nonlinearity is included in the model, hence the curved beam is suitable for large displacements. The equation of motion is derived by the principle of virtual work. The Ritz method is used for space discretization. Hierarchical higher order polynomial functions are used as shape functions for achieving better approximations of the displacement components. The derived beam model is validated by three-dimensional finite elements. Static deformations are analyses and the nonlinear algebraic system of equation is solved by Newton–Raphson's method. Prediction for the next point from the force–displacement curve is defined by the arc-length continuation method. The magnitude of the applied static load is assumed as parameter. Buckling, loss of stability and secondary branches are found, presented and analyzed.

2. Derivation of the equation of motion

A curved beam with rectangular cross section is considered (Fig. 1), where l is the length of the beam, b is the width and h is the thickness. R represents the radius of the arch. The material of the beam is assumed to be isotropic, homogeneous and elastic. r and θ are the polar coordinates in radial and circumferential directions, respectively, $r \in \left[R - \frac{h}{2}, \ldots, R + \frac{h}{2}\right]$ and $\theta \in \left[-\frac{l}{2R}, \ldots, \frac{l}{2R}\right]$.

The equation of motion is derived in polar coordinate system. The polar coordinate system is preferred for accurately representing the initial geometry of the beam. The displacements of the beam in radial and circumferential directions are expressed by the displacements on the middle line. Bernoulli–Euler's hypothesis is applied here for deriving the displacement components. It is assumed that the cross section does not deform and cross sections perpendicular to the middle line before deformation remain perpendicular to the middle line after deformation. The angle of rotation of the cross section is expressed by the derivative of the radial displacement on the middle line (Fig. 2).

Taking into account this assumption, the following expression for the displacement components is obtained [8]:

$$\begin{aligned} u_r(r,\theta,t) &= u_r^0(\theta,t), \\ u_\theta(r,\theta,t) &= \frac{r}{R}u_\theta^0(\theta,t) + \left(1-\frac{r}{R}\right)\frac{\partial u_r^0(\theta,t)}{\partial\theta}, \end{aligned} \tag{1}$$

where u_r denotes the radial displacement of the beam, u_θ is the circumferential displacement of the beam, u_r^0 and u_θ^0 are the radial and circumferential displacements on the middle line, i.e. $r = R$.

The nonlinear strain–displacement relations are derived from Green–Lagrange strain tensor expressed in cylindrical coordinate system, but using only the components related with radial and circumferential displacements. Assuming that $u_\theta \ll u_r$, the following expression for the circumferential strain is obtained [18]:

$$\varepsilon_\theta = \frac{u_r}{r} + \frac{1}{r}\frac{\partial u_\theta}{\partial\theta} + \frac{1}{2}\left(\frac{1}{r}\frac{\partial u_r}{\partial\theta}\right)^2 + \frac{1}{2}\left(\frac{u_r}{r}\right)^2 \tag{2}$$

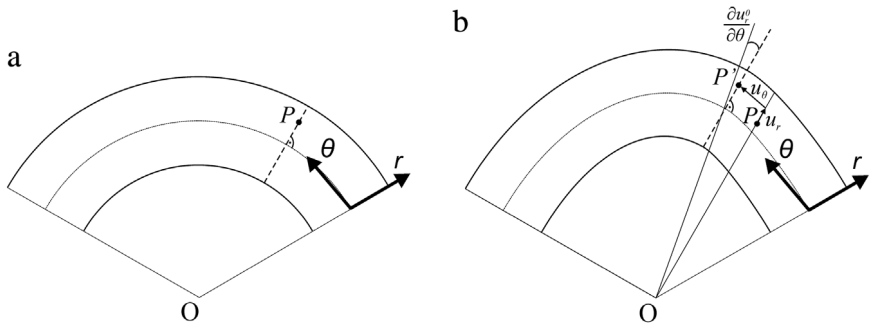

Fig. 2. Deformation of curved beam in polar coordinate systems by assuming Bernoulli–Euler's hypothesis. (a) Beam configuration before deformation, (b) beam after deformation.

From the displacement field (1), it can be verified that the shear strain $\gamma_{r\theta}$, which is given by the expression [18]:

$$\gamma_{r\theta} = \frac{1}{r}\frac{\partial u_r}{\partial \theta} + \frac{\partial u_\theta}{\partial r} - \frac{u_\theta}{r} = 0, \tag{3}$$

vanishes, which confirms that the displacement components satisfy Bernoulli–Euler's condition for zero shear strain. Hence, the only significant strain for the curved beam is the circumferential strain ε_θ.

A simplified form of Hooke's law is used to express the circumferential stress:

$$\sigma_\theta = E\varepsilon_\theta, \tag{4}$$

where E is the Young modulus of the material.

The equation of motion is derived by the principle of virtual work and discretized into a system of ordinary differential equations by the Ritz method. Accuracy is achieved by including higher order polynomials in the finite-dimensional subspace. This kind of discretization is widely known among engineers as p-version of the finite element method. The displacement components on the middle line are expressed by shape functions and generalized coordinates in a local coordinate system:

$$\begin{Bmatrix} u_r^0(\xi,t) \\ u_\theta^0(\xi,t) \end{Bmatrix} = \begin{bmatrix} \mathbf{N^r}(\xi)^{\mathrm{T}} & 0 \\ 0 & \mathbf{N^\theta}(\xi)^{\mathrm{T}} \end{bmatrix} \begin{Bmatrix} \mathbf{q_r}(t) \\ \mathbf{q_\theta}(t) \end{Bmatrix}, \tag{5}$$

where $\mathbf{N^r}(\xi)$ and $\mathbf{N^\theta}(\xi)$ are vectors of shape functions and $\mathbf{q_r}(t)$ and $\mathbf{q_\theta}(t)$ are the unknown vectors of generalized coordinates which depend on time t. $\xi \in [-1,\ldots,1]$ is the local coordinate, which has the following relation with the circumferential coordinate $\xi = \frac{2R}{l}\theta$.

The shape functions must satisfy the geometric boundary conditions. In this work, clamped-clamped boundary conditions are assumed, thus:

$$\begin{aligned} &u_r^0(\xi,t) = 0, \\ &\frac{\partial u_r^0(\xi,t)}{\partial \xi} = 0, \quad \text{for } \xi = \pm 1. \\ &u_\theta^0(\xi,t) = 0. \end{aligned} \tag{6}$$

The sets of shape functions used in previous works [19,20] are implemented here.

The equation of motion is derived by the principle of virtual work:

$$\delta W_V + \delta W_{in} + \delta W_E = 0, \tag{7}$$

where W_V, W_{in} and W_E are the virtual work of internal, inertia and external forces due to a virtual displacement $\delta\mathbf{d}$:

$$\delta\mathbf{d} = \begin{Bmatrix} \delta u_r \\ \delta u_\theta \end{Bmatrix}. \tag{8}$$

The variations of the work of internal, inertia and external forces are defined as:

$$\begin{aligned} \delta W_V &= -\int_V \delta\varepsilon_\theta \sigma_\theta dV, \\ \delta W_{in} &= -\int_V \rho\delta\mathbf{d}^{\mathrm{T}}\ddot{\mathbf{d}}dV, \\ \delta W_E &= \int_V \delta\mathbf{d}_0^{\mathrm{T}}\mathbf{f}_0 dV, \end{aligned} \tag{9}$$

where $\ddot{\mathbf{d}}$ is the acceleration vector of a point of the beam, $\mathbf{d}_0$ is the vector of displacement components on the middle line, ρ is the density of the beam, $\mathbf{f}_0$ represents external forces applied on the middle line.

By substituting Eq. (9) into (7), the following nonlinear system of ordinary differential equations is obtained:

$$\mathbf{M}\ddot{\mathbf{q}}(t) + \mathbf{K}(\mathbf{q}(t))\,\mathbf{q}(t) = \mathbf{f}(t) \tag{10}$$

where $\mathbf{M}$ represents the mass matrix, which results from the inertia forces, $\mathbf{K}(\mathbf{q}(t))$ represents the stiffness matrix which depends on the vector of generalized coordinates $\mathbf{q}(t)$. $\mathbf{f}(t)$ is the vector of generalized external forces. The structure of the mass and stiffness matrices is given in details in Appendix.

3. Numerical methods for static analysis

The equilibrium equation under the influence of static loads has the following form:

$$\mathbf{K}(\mathbf{q})\,\mathbf{q} = a\mathbf{f}, \tag{11}$$

where a is the load parameter and the vector of generalized coordinates $\mathbf{q}$ does not depend on time. The magnitude of the static force is assumed as parameter and the algebraic system (11) is solved by Newton–Raphson's method. Prediction for the next point in the parametric domain is defined by the arc-length continuation method [21].

Eq. (11) can be written in the following form:

$$\mathbf{g}(\mathbf{q}, a) = 0 \tag{12}$$

where

$$\mathbf{g}(\mathbf{q}, a) = \mathbf{K}(\mathbf{q})\,\mathbf{q} - a\mathbf{f},\ \mathbf{g} : \mathrm{R}^{n+1} \to \mathrm{R}^{n} \tag{13}$$

The arc-length continuation method is predictor–corrector method where one follows a branch of solutions. The method is suitable to pass turning points (saddle–node bifurcation points) and by additional computations allows one to investigate the stability of the solution, to determine bifurcation points and to follow secondary branches.

Stability of the solution is determined by computing the eigenvalues of the Jacobian of (12). Suppose that $(\mathbf{q}_0, a_0)$ is solution of (12) and the Jacobian is defined by:

$$\mathbf{J} = \frac{\partial \mathbf{g}}{\partial \mathbf{q}}(\mathbf{q}_0, a_0) \tag{14}$$

The stability is determined by the real parts of the eigenvalues μ_i of the evaluated Jacobian at the solution $(\mathbf{q}_0, a_0)$ in the following way [22]:

$Re(\mu_i) < 0$ for all i implies asymptotic stability,

$Re(\mu_k) > 0$ for one or more k implies instability.

Bifurcation points are determined taking into account that in the $\mathbf{q} - a$ state space, the point $(\mathbf{q}_0, a_0)$ is bifurcation point if the following conditions are satisfied:

$$\begin{aligned} \mathbf{g}(\mathbf{q}_0, a_0) &= 0 \\ \frac{\partial \mathbf{g}}{\partial \mathbf{q}}(\mathbf{q}_0, a_0) &= 0 \end{aligned} \tag{15}$$

The first equation ensures that the point $(\mathbf{q}_0, a_0)$ is solution of the equilibrium equation, and the second equation ensures that this point is a nonhyperbolic fixed point [22].

The conditions (15) include the so called saddle–node bifurcation points, from which there is no secondary branch of solutions. The saddle–node bifurcation points are also known as folds, or turning points.

Secondary branches are computed from the solution where bifurcation point (but not turning point) is found. By the implicit function theorem, in a neighborhood of the bifurcation point, the equilibrium equation has more than one solution. At the bifurcation point, at least one eigenvalue of the Jacobian has zero real part. The corresponding eigenvector is used to determine the direction of the predictor in the continuation method. In this way, the corrector step ensures that new solution belong to the secondary branch of solutions.

4. Validation of the model

The model is validated by comparing the natural frequencies and static displacements of equivalent curved beam structure discretized with three-dimensional finite elements. The material of the beam is assumed to be aluminium with the following properties: E = 70 GPa, $\rho = 2778\mathrm{kg/m}^3$, $\nu = 0.34$. The length of the beam is considered to be $l = 0.58$ m, the width $b = 0.02$ m, the thickness $h = 0.002$ m, and different curvature of the beam are assumed. Clamped-clamped boundary conditions are considered. 15 shape functions are used for each displacement component, i.e. the degrees of freedom are 30.

The natural frequencies are compared with results obtained by finite element software Elmer [23]. Elmer is finite element software which employs three-dimensional finite elements for the nonlinear equation of elasticity. The three-dimensional

Table 1
Natural frequencies (rad/s) of semi-circular arc beam with clamped-clamped boundary conditions.

Mode	Elmer	Beam model 20 DOF	Beam model 30 DOF	Diff. between Elmer and beam 20 DOF %	Diff. between Elmer and beam 30 DOF %
1	375.74	372.80	372.80	0.79	0.79
2	826.23	820.58	820.57	0.69	0.69
3	1534.04	1527.86	1523.73	0.41	0.68
4	2355.01	2361.84	2339.54	0.28	0.66
5	3406.12	3889.47	3383.14	14.18	0.68
6	4575.50	5701.99	4550.50	24.61	0.56

Table 2
Static displacements of curved beam with $R = 5$ m. Comparison of the current beam model with Elmer.

Force [N]	Elmer [m]	Beam model [m]	Diff. %
−5	−8.150E−04	−8.155E−04	0.06
−8.6	−2.740E−03	−2.795E−03	1.99
−8.7	−1.312E−02	−1.317E−02	0.38
−10	−1.342E−02	−1.347E−02	0.37
−20	−1.484E−02	−1.488E−02	0.21
−30	−1.570E−02	−1.571E−02	0.11
−40	−1.633E−02	−1.634E−02	0.03
−50	−1.686E−02	−1.685E−02	0.04

equation of elasticity does not consider any simplifications, like the Bernoulli–Euler hypothesis, or it does not neglect any of the nonlinear terms. Thus, the comparison of the beam model with the three-dimensional equation of elasticity presents reliable validation of the model. Convergence with the size of the mesh is performed for guaranteeing accurate results.

A fine mesh of quadratic tetrahedrons is generated by Gmsh [24]. The resulting system has about 1.8 million DOF. The resulting large-scale system is solved on parallel processors using Mumps library (MUltifrontal Massively Parallel Solver) [25]. It was verified, by reducing the size of the tetrahedrons, that the results obtained by the large-scale model are converged.

The natural frequencies of semi-circular arc are given in Table 1. The results confirm that accurate results are achieved by the derived beam model in polar coordinate system. The natural modes of vibration are shown in Fig. 3.

Further to validate the curved beam model, including the geometrically nonlinear terms, a static force is applied on the middle of the beam in direction to the center of the polar coordinate system. A beam with $R = 5$ m and the same material and geometrical properties is considered. The magnitude of the static force is considered as parameter, and the nonlinear algebraic equation of equilibrium is solved in parametric domain by Newton–Raphson's method and by the arc-length continuation method. For certain values of the load parameter, the displacement in radial direction is computed by the three-dimensional beam structure and Elmer software. The results are presented in Table 2 and the corresponding force–displacement curve is shown in Fig. 4. The deformed beam structure is presented in Fig. 5, obtained by the current beam model and Elmer.

The results confirm that the derived nonlinear beam model in polar coordinate system gives very close results to the three-dimensional elasticity equation of equilibrium applied to equivalent curved beam structure. Furthermore, the buckling of the curved beam, which becomes for static forces between −8.6 and −8.7 N is successfully modeled. The Elmer software does not provide parametric analysis, thus the results were compared for certain fixed values of the static force.

5. Static analysis of curved beams

Curved beams with different radius of the arch are compared and investigated. Static force with uniformly distributed load is applied on the beam in radial direction. The magnitude of the force is assumed as parameter and the results are presented in force–displacement diagrams. The aim of the analysis is to investigate the influence of the applied force on the displacements of the beam, to determine the critical values where buckling appears, to determine bifurcation points, stability of the equilibrium solution and to find the secondary branches of solutions. Furthermore, the aim is to investigate the influence of the radius of the arch on the displacements of the beam.

Curved beams with fixed length $l = 0.58$ m are investigated. Three different radii of the arch are considered: $R = 10$ m, $R = 5$ m and $R = 3$m. The total magnitude of the uniformly distributed applied forces is assumed to vary from −70 to 70 N. The arc-length continuation method is started with parametric load with magnitude zero. Then, it is increased in positive direction to obtain the force–displacement curves that correspond to positive load. The continuation method is started again from parametric load with zero magnitude, but the parameter is increased in negative direction to obtain the force–displacement curves that correspond to negative load. The parametric analysis of the three curved beams is presented in Fig. 6.

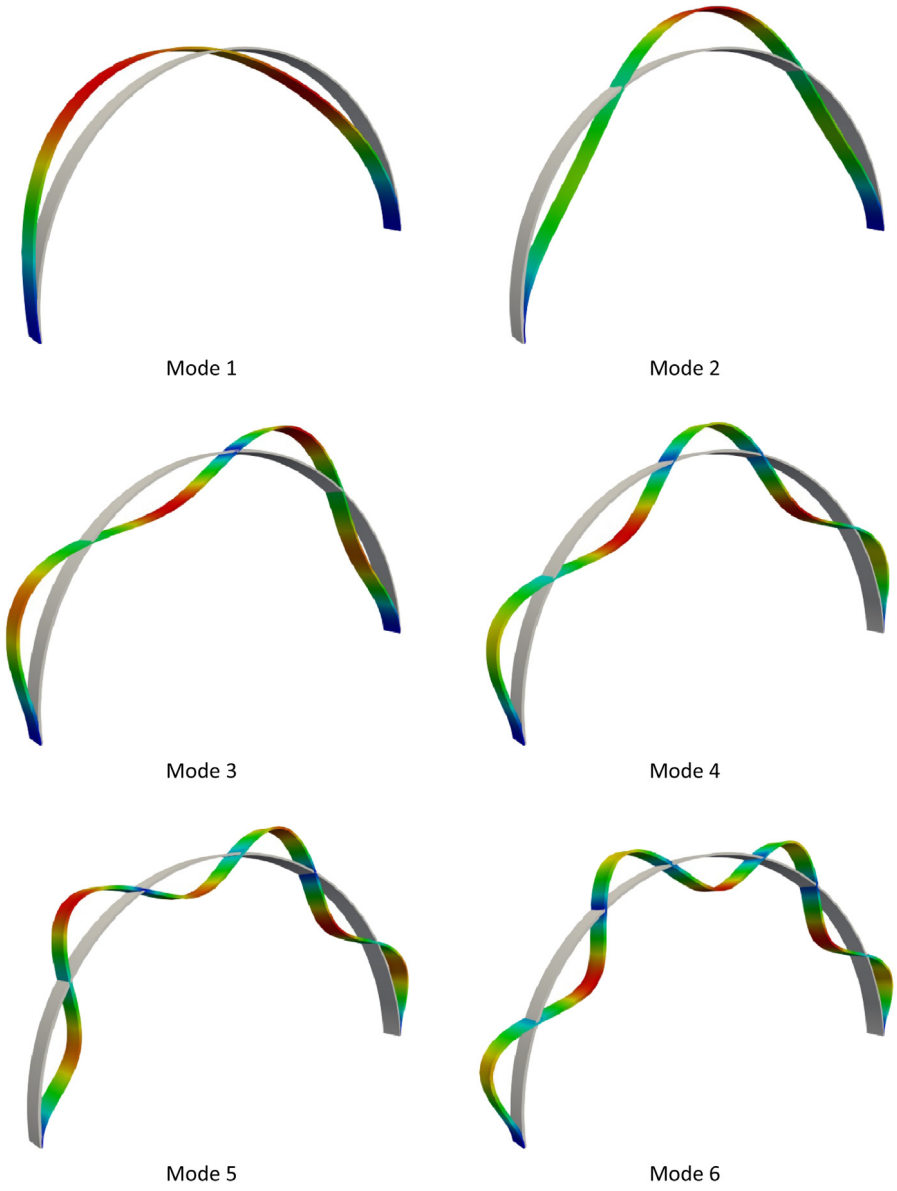

Fig. 3. Mode shapes of curved beam corresponding to the natural frequencies given in Table 1. The results are obtained by three-dimensional FEM with Elmer, equivalent mode shapes are obtained by the beam model.

It is seen that when the force is positive, the behavior of the beam is straightforward, there is no buckling, there is no loss of stability, neither secondary branches. Increasing the load parameter leads to bigger displacements of the beam, but the "force–displacement" relations are nonlinear.

More interesting results appear when the applied force is negative. In this case, for certain values of the applied force, buckling of the beam appears, bifurcation points and secondary branches also exist.

Fig. 6 presents the force–displacement diagram of the three curved beams under study. Subcritical pitchfork bifurcation points and saddle–node bifurcation points are found. It is important to note that the pitchfork bifurcation points are obtained before the saddle–node bifurcation points. Hence, the equilibrium of the solution loses stability after the bifurcation point. The main branch of the solutions, between the bifurcation point and the saddle–node bifurcation point is unstable. This means that when external forces are applied in real experiment, the buckling will appear immediately after the bifurcation point and before the saddle–node bifurcation point (Fig. 7). The beam will deform with shape that correspond to the stable solution after the second saddle–node bifurcation point. If the force is decreased in buckled configuration, the beam will reduce its displacement significantly, after the saddle–node bifurcation point.

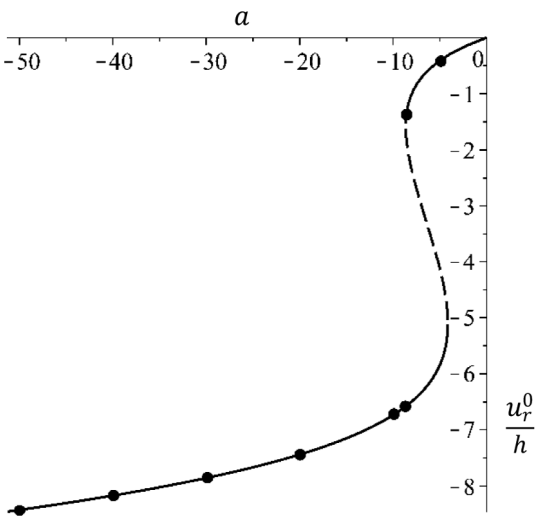

Fig. 4. Static displacements of curved beam with $R = 5$. Dots represent the values obtained by Elmer.

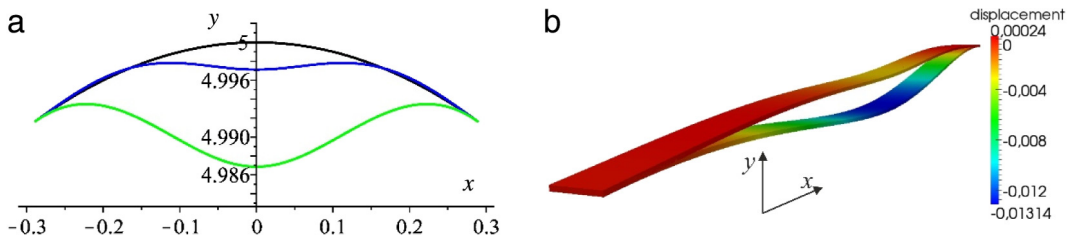

Fig. 5. Deformed shape of curved beam due to static forces. (a) Beam model: undeformed beam, deformation due to static forces $f_y = -8.6$, $f_y = -8.7$ N, (b) Deformations of beam structure obtained by Elmer for $f_r = -8.6$ and $f_r = -8.7$, x and y are the Cartesian coordinates.

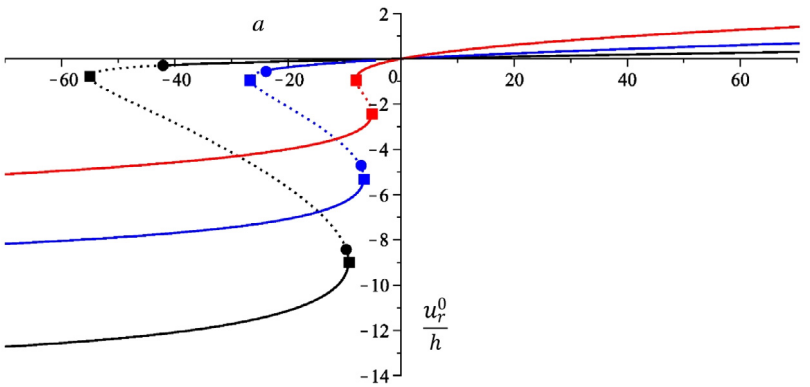

Fig. 6. Static displacements of curved beam due to uniformly distributed force in radial direction. Red – $R = 10$ m, blue – $R = 5$ m, black – $R = 3$ m. ■ – saddle–node bifurcation (turning point), • – subcritical pitchfork bifurcation point. Displacements are measured in the middle of the beam ($\xi = 0$). (For interpretation of the references to colour in this figure legend, the reader is referred to the web version of this article.)

There are two unstable secondary branches which arise from the pitchfork bifurcation point. In Fig. 7 they are not visible, because the deformed shapes from the secondary branches are symmetric with respect to the middle of the beam and the magnitude of displacement is measured in the middle of the beam ($\xi = 0$). The unstable branches are visible in Fig. 8, where the magnitude of the deformed beam is measured for $\xi = 0.5$.

Fig. 9 shows that for certain values of the applied force, there are three solutions from the main branch and two solutions from the secondary branches. Fig. 9 shows the displacement configurations of the beam for applied uniformly distributed

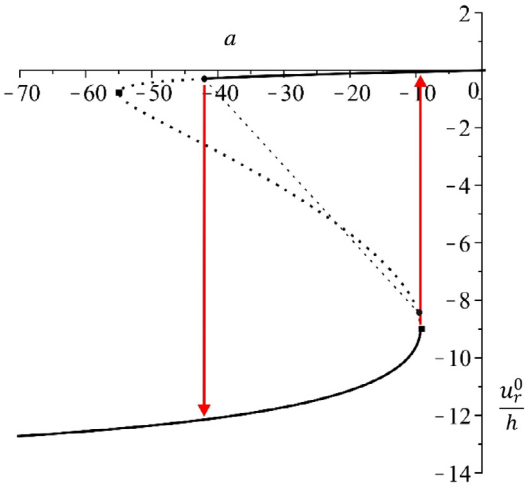

Fig. 7. Buckling of curved beam, $R = 3$ m, ■ – saddle–node bifurcation (turning point), • – subcritical pitchfork bifurcation point.

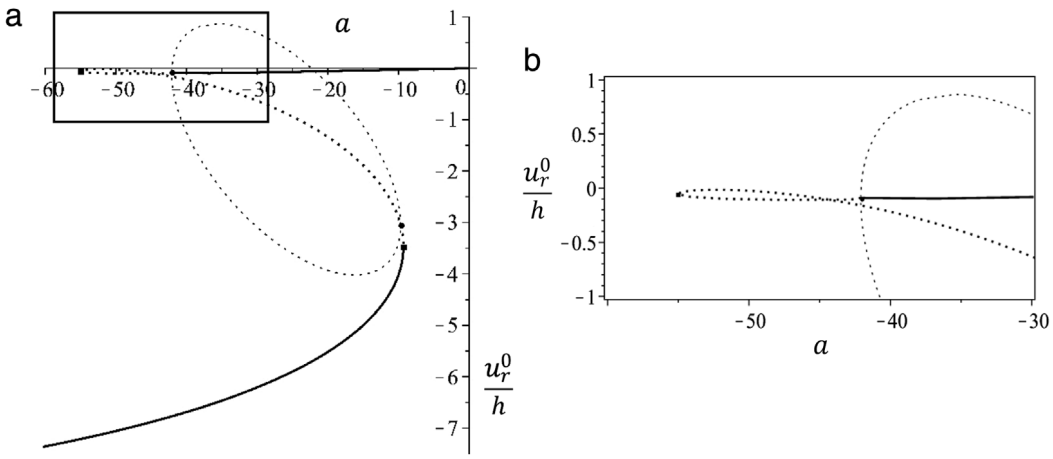

Fig. 8. (a) Static displacements of curved beam due to uniformly distributed force in radial direction, $R = 3$ m. ($\xi = 0.5$), (b) zoomed area of (a).

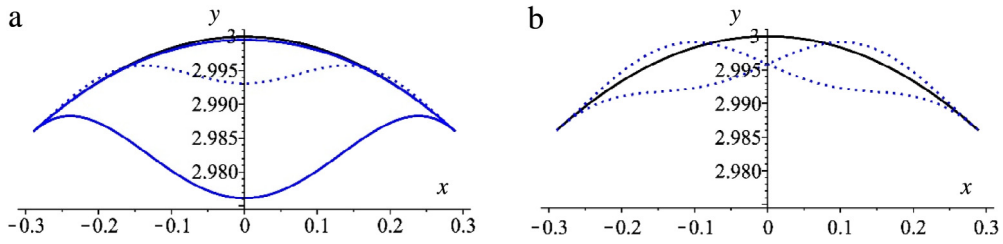

Fig. 9. Displacements from the (a) main and (b) secondary branch of curved beam ($R = 3$ m) due to uniformly distributed force $F = 35$ N/m. ▬ undeformed beam, ▬ deformed beam, stable solution, ••• deformed beam, unstable solution.

force of 35 N/m. The main branch presents symmetrical solutions with respect to the middle of the beam. It has stable solution with small displacements, unstable solution with bigger displacements, which is between the two saddle–node bifurcation points and stable solution with large displacements, which appears after buckling. The solutions from the secondary branch are unstable and non-symmetric with respect to the middle of the beam. It is important to note that secondary branches were not found when the applied force was a point force on the middle of the beam.

6. Conclusions

The equation of motion of curved beams is derived in polar coordinate system by the principle of virtual work, assuming Bernoulli–Euler's theory and including geometrical type of nonlinearity. It is discretized by Ritz method by using hierarchical higher order polynomial functions as shape functions. The derived model is validated by three-dimensional finite elements based on three-dimensional equation of elasticity. It is shown that accurate results of curved structures can be achieved by the proposed beam model with few degrees of freedom.

Static analysis is performed in the parametric domain, assuming the magnitude of the applied force as parameter. Beams with different curvatures are analyzed. Stability of the solution is determined, bifurcation points are found and the corresponding secondary branches are obtained and presented. It is shown that buckling can appear before the saddle–node bifurcation point from the "force–displacement" due to lose of stability of the solution.

Appendix

Here are presented the mass and the stiffness matrices of the curved beam model introduced in Section 2.

To simplify the derivation of the stiffness matrix, the circumferential strain, given in Eq. (2), is separated into linear and nonlinear parts:

$$\varepsilon_\theta = \varepsilon_L + \varepsilon_{NL} \tag{A.1}$$

where

$$\varepsilon_L = \frac{1}{R}\frac{\partial u_\theta^0}{\partial \theta} + \left(\frac{1}{r} - \frac{1}{R}\right)\frac{\partial^2 u_r^0}{\partial \theta^2} + \frac{1}{r}u_r^0 \tag{A.2}$$

$$\varepsilon_{NL} = \frac{1}{2r^2}\left(\frac{\partial u_r^0}{\partial \theta}\right)^2 + \frac{1}{2r^2}u_r^{0^2} \tag{A.3}$$

The stiffness matrix can be separated into matrix that is constant, two matrices that depend linearly on the vector of generalized coordinates and one matrix that depends quadratically on the vector of generalized coordinates. It is written in the following form:

$$\mathbf{K}(\mathbf{q}) = \mathbf{K}1 + \mathbf{K}2(\mathbf{q}) + \mathbf{K}3(\mathbf{q}) + \mathbf{K}4(\mathbf{q}, \mathbf{q}) \tag{A.4}$$

where each of the sub-matrices is defined by the following expressions:

$$\int_V \delta\varepsilon_L E \varepsilon_L dV = (\delta\mathbf{q})^{\mathrm{T}}\mathbf{K}1\mathbf{q} \tag{A.5}$$

$$\int_V \delta\varepsilon_L E \varepsilon_{NL} dV = (\delta\mathbf{q})^{\mathrm{T}}\mathbf{K}2(\mathbf{q})\,\mathbf{q} \tag{A.6}$$

$$\int_V \delta\varepsilon_{NL} E \varepsilon_L dV = (\delta\mathbf{q})^{\mathrm{T}}\mathbf{K}3(\mathbf{q})\,\mathbf{q} \tag{A.7}$$

$$\int_V \delta\varepsilon_{NL} E \varepsilon_{NL} dV = (\delta\mathbf{q})^{\mathrm{T}}\mathbf{K}4(\mathbf{q}, \mathbf{q})\,\mathbf{q} \tag{A.8}$$

The stiffness matrix of constant terms has the following structure:

$$\mathbf{K}1 = \begin{bmatrix} \mathbf{K}1_{11} & \mathbf{K}1_{12} \\ \mathbf{K}1_{12}^{\mathrm{T}} & \mathbf{K}1_{22} \end{bmatrix} \tag{A.9}$$

where each of the sub-matrices is expressed by the vectors of shape functions. The transformation from global to local coordinates is presented only for the stiffness matrix of constant terms. Vectors $\overline{\mathbf{N}}^{\mathbf{r}}(\theta)$ and $\overline{\mathbf{N}}^{\boldsymbol{\theta}}(\theta)$ denote the vectors of shape functions, written in global coordinate system, while vectors $\mathbf{N}^{\mathbf{r}}(\xi)$ and $\mathbf{N}^{\boldsymbol{\theta}}(\xi)$ denote the vectors of shape functions, written in local coordinate system.

$$\begin{aligned}
\mathbf{K}1_{11} &= E\int_V \left(\frac{1}{r} - \frac{1}{R}\right)^2 \frac{\partial^2 \overline{\mathbf{N}}^{\mathbf{r}}(\theta)}{\partial\theta^2}\frac{\partial^2 \overline{\mathbf{N}}^{\mathbf{r}}(\theta)^{\mathrm{T}}}{\partial\theta^2} dV + E\int_V \frac{1}{r}\left(\frac{1}{r} - \frac{1}{R}\right)\frac{\partial^2 \overline{\mathbf{N}}^{\mathbf{r}}(\theta)}{\partial\theta^2}\overline{\mathbf{N}}^{\mathbf{r}}(\theta)^{\mathrm{T}} dV \\
&\quad + E\int_V \frac{1}{r}\left(\frac{1}{r} - \frac{1}{R}\right)\overline{\mathbf{N}}^{\mathbf{r}}(\theta)\frac{\partial^2 \overline{\mathbf{N}}^{\mathbf{r}}(\theta)^{\mathrm{T}}}{\partial\theta^2} dV + E\int_V \frac{1}{r^2}\overline{\mathbf{N}}^{\mathbf{r}}(\theta)\overline{\mathbf{N}}^{\mathbf{r}}(\theta)^{\mathrm{T}} dV \\
&= \frac{8EbR^3}{l^3}\int_{R-\frac{h}{2}}^{R+\frac{h}{2}} r\left(\frac{1}{r} - \frac{1}{R}\right)^2 dr \int_{-1}^{1} \frac{\partial^2 \mathbf{N}^{\mathbf{r}}(\xi)}{\partial\xi^2}\frac{\partial^2 \mathbf{N}^{\mathbf{r}}(\xi)^{\mathrm{T}}}{\partial\xi^2} d\xi \\
&\quad + \frac{2EbR}{l}\int_{R-\frac{h}{2}}^{R+\frac{h}{2}} \left(\frac{1}{r} - \frac{1}{R}\right) dr \int_{-1}^{1} \frac{\partial^2 \mathbf{N}^{\mathbf{r}}(\xi)}{\partial\xi^2}\mathbf{N}^{\mathbf{r}}(\xi)^{\mathrm{T}} d\xi
\end{aligned}$$

$$+ \quad \frac{2EbR}{l}\int_{R-\frac{h}{2}}^{R+\frac{h}{2}}\left(\frac{1}{r}-\frac{1}{R}\right)dr\int_{-1}^{1}\mathbf{N}^{\mathbf{r}}(\xi)\frac{\partial^2\mathbf{N}^{\mathbf{r}}(\xi)^{\mathrm{T}}}{\partial\xi^2}d\xi+\frac{Ebl}{2R}\int_{R-\frac{h}{2}}^{R+\frac{h}{2}}\frac{1}{r}dr\int_{-1}^{1}\mathbf{N}^{\mathbf{r}}(\xi)\mathbf{N}^{\mathbf{r}}(\xi)^{\mathrm{T}}d\xi$$

$$\mathbf{K}1_{12}=E\int_V\frac{1}{R}\left(\frac{1}{r}-\frac{1}{R}\right)\frac{\partial^2\overline{\mathbf{N}}^{\mathbf{r}}(\theta)}{\partial\theta^2}\frac{\partial\overline{\mathbf{N}}^{\boldsymbol{\theta}}(\theta)^{\mathrm{T}}}{\partial\theta}dV+E\int_V\frac{1}{Rr}\overline{\mathbf{N}}^{\mathbf{r}}(\theta)\frac{\partial\overline{\mathbf{N}}^{\boldsymbol{\theta}}(\theta)^{\mathrm{T}}}{\partial\theta}dV$$

$$=\frac{4EbR^2}{l^2}\int_{R-\frac{h}{2}}^{R+\frac{h}{2}}\frac{r}{R}\left(\frac{1}{r}-\frac{1}{R}\right)dr\int_{-1}^{1}\frac{\partial^2\mathbf{N}^{\mathbf{r}}(\xi)}{\partial\xi^2}\frac{\partial\mathbf{N}^{\boldsymbol{\theta}}(\xi)^{\mathrm{T}}}{\partial\xi}d\xi+\frac{Eb}{R}\int_{R-\frac{h}{2}}^{R+\frac{h}{2}}dr\int_{-1}^{1}\mathbf{N}^{\mathbf{r}}(\xi)\frac{\partial\mathbf{N}^{\boldsymbol{\theta}}(\xi)^{\mathrm{T}}}{\partial\xi}d\xi$$

$$\mathbf{K}1_{22}=E\int_V\frac{1}{R^2}\frac{\partial\overline{\mathbf{N}}^{\boldsymbol{\theta}}(\theta)}{\partial\theta}\frac{\partial\overline{\mathbf{N}}^{\boldsymbol{\theta}}(\theta)^{\mathrm{T}}}{\partial\theta}dV=\frac{2Eb}{Rl}\int_{R-\frac{h}{2}}^{R+\frac{h}{2}}rdr\int_{-1}^{1}\frac{\partial\mathbf{N}^{\boldsymbol{\theta}}(\xi)}{\partial\xi}\frac{\partial\mathbf{N}^{\boldsymbol{\theta}}(\xi)^{\mathrm{T}}}{\partial\xi}d\xi$$

The $\mathbf{K}2(\mathbf{q})$ matrix that depends linearly on the vector of generalized coordinates has the following form:

$$\mathbf{K}2(\mathbf{q})=\begin{bmatrix}\mathbf{K}2_{11}(\mathbf{q_r}) & 0\\ \mathbf{K}2_{21}(\mathbf{q_r}) & 0\end{bmatrix} \tag{A.10}$$

where

$$\mathbf{K}2_{11}(\mathbf{q_r})=\frac{1}{2}E\int_V\frac{1}{r^2}\left(\frac{1}{r}-\frac{1}{R}\right)\frac{\partial^2\overline{\mathbf{N}}^{\mathbf{r}}(\theta)}{\partial\theta^2}\frac{\partial\overline{\mathbf{N}}^{\mathbf{r}}(\theta)^{\mathrm{T}}}{\partial\theta}\frac{\partial u_r^0(\theta)}{\partial\theta}dV$$
$$+\frac{1}{2}E\int_V\frac{1}{r^2}\left(\frac{1}{r}-\frac{1}{R}\right)\frac{\partial^2\overline{\mathbf{N}}^{\mathbf{r}}(\theta)}{\partial\theta^2}\overline{\mathbf{N}}^{\mathbf{r}}(\theta)^{\mathrm{T}}u_r^0(\theta)\,dV$$
$$+\frac{1}{2}E\int_V\frac{1}{r^3}\overline{\mathbf{N}}^{\mathbf{r}}(\theta)\frac{\partial\overline{\mathbf{N}}^{\mathbf{r}}(\theta)^{\mathrm{T}}}{\partial\theta}\frac{\partial u_r^0(\theta)}{\partial\theta}dV+\frac{1}{2}E\int_V\frac{1}{r^3}\overline{\mathbf{N}}^{\mathbf{r}}(\theta)\overline{\mathbf{N}}^{\mathbf{r}}(\theta)^{\mathrm{T}}u_r^0(\theta)\,dV$$

$$\mathbf{K}2_{21}(\mathbf{q_r})=\frac{1}{2R}E\int_V\frac{1}{r^2}\frac{\partial\overline{\mathbf{N}}^{\boldsymbol{\theta}}(\theta)}{\partial\theta}\overline{\mathbf{N}}^{\mathbf{r}}(\theta)^{\mathrm{T}}u_r^0(\theta)\,dV+\frac{1}{2R}E\int_V\frac{1}{r^2}\frac{\partial\overline{\mathbf{N}}^{\boldsymbol{\theta}}(\theta)}{\partial\theta}\frac{\partial\overline{\mathbf{N}}^{\mathbf{r}}(\theta)^{\mathrm{T}}}{\partial\theta}\frac{\partial u_r^0(\theta)}{\partial\theta}dV$$

The matrix $\mathbf{K}3(\mathbf{q})$ has the following relation with matrix $\mathbf{K}2(\mathbf{q})$, which used in the model:

$$\mathbf{K}3(\mathbf{q})=2\mathbf{K}2(\mathbf{q})^{\mathrm{T}} \tag{A.11}$$

The quadratically dependent on the vector of generalized coordinates matrix $\mathbf{K}4(\mathbf{q},\mathbf{q})$ has the following structure:

$$\mathbf{K}4(\mathbf{q},\mathbf{q})=\begin{bmatrix}\mathbf{K}4_{11}(\mathbf{q_r}) & 0\\ 0 & 0\end{bmatrix} \tag{A.12}$$

where

$$\mathbf{K}4_{11}(\mathbf{q_r})=\frac{1}{2}E\int_V\frac{1}{r^4}\frac{\partial\overline{\mathbf{N}}^{\mathbf{r}}(\theta)}{\partial\theta}\frac{\partial\overline{\mathbf{N}}^{\mathbf{r}}(\theta)^{\mathrm{T}}}{\partial\theta}\left(\frac{\partial u_r^0(\theta)}{\partial\theta}\right)^2dV+\frac{1}{2}E\int_V\frac{1}{r^4}\frac{\partial\overline{\mathbf{N}}^{\mathbf{r}}(\theta)}{\partial\theta}\frac{\partial\overline{\mathbf{N}}^{\mathbf{r}}(\theta)^{\mathrm{T}}}{\partial\theta}u_r^0(\theta)^2dV$$
$$+\frac{1}{2}E\int_V\frac{1}{r^4}\overline{\mathbf{N}}^{\mathbf{r}}(\theta)\overline{\mathbf{N}}^{\mathbf{r}}(\theta)^{\mathrm{T}}\left(\frac{\partial u_r^0(\theta)}{\partial\theta}\right)^2dV+\frac{1}{2}E\int_V\frac{1}{r^4}\overline{\mathbf{N}}^{\mathbf{r}}(\theta)\overline{\mathbf{N}}^{\mathbf{r}}(\theta)^{\mathrm{T}}u_r^0(\theta)^2dV$$

The mass matrix has the following structure:

$$\mathbf{M}=\begin{bmatrix}\mathbf{M}_{11} & \mathbf{M}_{12}\\ \mathbf{M}_{12}^{\mathrm{T}} & \mathbf{M}_{22}\end{bmatrix} \tag{A.13}$$

where

$$\mathbf{M}_{11}=\rho\int_V\overline{\mathbf{N}}^{\mathbf{r}}(\theta)\overline{\mathbf{N}}^{\mathbf{r}}(\theta)^{\mathrm{T}}dV+\rho\int_V\left(1-\frac{r}{R}\right)^2\frac{\partial\overline{\mathbf{N}}^{\mathbf{r}}(\theta)}{\partial\theta}\frac{\partial\overline{\mathbf{N}}^{\mathbf{r}}(\theta)^{\mathrm{T}}}{\partial\theta}dV$$
$$\mathbf{M}_{12}=\rho\int_V\frac{r}{R}\left(1-\frac{r}{R}\right)\frac{\partial\overline{\mathbf{N}}^{\mathbf{r}}(\theta)}{\partial\theta}\overline{\mathbf{N}}^{\boldsymbol{\theta}}(\theta)^{\mathrm{T}}dV$$
$$\mathbf{M}_{22}=\rho\int_V\frac{r^2}{R^2}\overline{\mathbf{N}}^{\boldsymbol{\theta}}(\theta)\overline{\mathbf{N}}^{\boldsymbol{\theta}}(\theta)^{\mathrm{T}}dV.$$

References

[1] A. Boresi, O. Sidebottom, Avanced Mechanics of Materials, John Wiley, New York, 1985.
[2] B. Lee, T. Lee, D. Ahn, Free vibrations of horizontally curved beams with unsymmetric axes in Cartesian coordinates, KSCE J. Civil Eng. 7 (2) (2003) 147–152.

[3] B. Lee, T. Lee, T. Ahn, Free vibrations of arches with inclusion of axial extension, shear deformation and rotatory inertia in Cartesian coordinates, KSCE J. Civil Eng. 8 (1) (2004) 43–48.
[4] M. Wang, Y. Liu, Elasticity solutions for orthotropic functionally graded curved beams, Eur. J. Mech. A Solids 37 (2013) 8–16.
[5] F. Fraternali, S. Spadea, L. Ascione, Buckling behavior of curved composite beams with different elastic response in tension and compression, Compos. Struct. 100 (2013) 280–289.
[6] P. Ribeiro, A p-version, first order shear deformation, finite element for geometrically non-linear vibration of curved beams, Internat. J. Numer. Methods Engrg. 61 (5) (2004) 2696–2715.
[7] K. Hsiao, R. Yang, A co-rotational formulation for nonlinear dynamics analysis of curved Euler beam, Comput. Struct. 54 (1995) 1091–1097.
[8] S. Lenci, F. Clementi, Simple mechanical model of curved beams by a 3D approach, J. Eng. Mech. 135 (2009) 597–613.
[9] P. Ribeiro, E. Manoach, The effect of temperature on the large amplitude vibrations of curved beams, J. Sound Vib. 285 (4–5) (2005) 1093–1107.
[10] M. Ganapathi, O. Polit, Dynamic characteristics of curved nanobeams using nonlocal higher-order curved beam theory, Physica E 91 (2017) 190–202.
[11] W. Li, H. Ma, W. Gao, Geometrically exact curved beam element using internal force field defined in deformed configuration, Int. J. Non-Linear Mech. 89 (2017) 116–126.
[12] D. Zulli, R. Alaggio, F. Benedettini, Non-linear dynamics of curved beams. Part 1: Formulation, Int. J. Non-Linear Mech. 44 (2009) 623–629.
[13] M. Ishaquddin, P. Raveendranath, J. Reddy, Coupled polynomial field approach for elimination of flexure and torsion locking phenomena in the Timoshenko and Euler–Bernoulli curved beam elements, Finite Elem. Anal. Des. 65 (2013) 17–31.
[14] M. Ishaquddin, P. Raveendranath, J. Reddy, Efficient coupled polynomial interpolation scheme for out-of-plane free vibration analysis of curved beams, Finite Elem. Anal. Des. 110 (2016) 58–66.
[15] I. Tsiptsis, E. Sapountzakis, Isogeometric analysis for the dynamic problem of curved structures including warping effects, Mech. Based Des. Struct. Mach. (2017) 1–19.
[16] O. Rahmani, S. Hosseini, I. Ghoytasi, H. Golmohammadi, Buckling and free vibration of shallow curved micro/nano-beam based on strain gradient theory under thermal loading with temperature-dependent properties, Appl. Phys. A 123 (2017) 4.
[17] A. Pydah, A. Sabale, Static analysis of bi-directional functionally graded curved beams, Compos. Struct. 160 (15) (2017) 867–876.
[18] J.N. Reddy, An Introduction to Continuum Mechanics, Cambridge University Press, New York, 2013.
[19] S. Stoykov, P. Ribeiro, Nonlinear forced vibrations and static deformations of 3d beams with rectangular cross section: The influence of warping, shear deformation and longitudinal displacements, Int. J. Mech. Sci. 52 (2010) 1505–1521.
[20] S. Stoykov, E. Manoach, S. Margenov, An efficient 3D numerical beam model based on cross sectional analysis and Ritz approximations, ZAMM J. Appl. Math. Mech. 96 (2016) 791–812.
[21] A. Nayfeh, B. Balachandran, Applied Nonlinear Dynamics: Analytical Computational and Experimental Methods, John Wiley & Sons, Inc., New York, 1995.
[22] R. Seydel, Practical Bifurcation and Stability Analysis, third ed., Springer, New York, 2010.
[23] Elmer web site: www.csc.fi/elmer (last time visited 01/06/2017).
[24] C. Geuzaine, J.-F. Remacle, Gmsh: a three-dimensional finite element mesh generator with built-in pre- and post-processing facilities, Internat. J. Numer. Methods Engrg. 79 (2009) 1309–1331.
[25] P.R. Amestoy, A. Guermouche, J.Y. L'Excellent, S. Pralet, Hybrid scheduling for the parallel solution of linear systems, Parallel Comput. 32 (2006) 136–156.